European Journal of Medicinal Chemistry 46 (2011) 1638–1647

Contents lists available at ScienceDirect

European Journal of Medicinal Chemistry

journal homepage: http://www.elsevier.com/locate/ejmech

Original article

Transition metal complexes of 2, 6-di ((phenazonyl-4-imino) methyl)-4-methylphenol: Structure and biological evaluation

Hongyan Liu [a], Xiaoyan Shi [b], Min Xu [a], Zhengpeng Li [a], Liang Huang [a], Decheng Bai [c], ZhengZhi Zeng [a,*]

[a] Key Laboratory of Nonferrous Metals Chemistry and Resources Utilization of Gansu Province, College of Chemistry and Chemical Engineering, Lanzhou University, Lanzhou 730000, PR China
[b] Department of Prosthodontics, School of Stomatology, Lanzhou University, Lanzhou 730000, PR China
[c] Key Laboratory of Pre-clinical Study for New Drugs of Gansu Province, Basic Medical College, Lanzhou University, Lanzhou 730000, PR China

ARTICLE INFO

Article history:
Received 4 November 2010
Received in revised form
26 December 2010
Accepted 8 February 2011
Available online 15 February 2011

Keywords:
Transition metal complexes
Bovine serum albumin binding
DNA interaction
Cleavage

ABSTRACT

A symmetric ligand 2, 6-di ((phenazonyl-4-imino)methyl)-4-methylphenol (Dpmp) and its cobalt dinuclear complex $(Co_2(Dpmp)_2(NO3)_2(H_2O)_2\cdot NO3\cdot EtOH$, (**1**) and zinc mononuclear complex Zn(Dpmp) $(NO_3)_2$, (**2**) have been prepared. The crystal structures were determined by single-crystal X-ray diffraction. The biological activity has been evaluated by examining their anti-oxidative activity and ability to bind to bovine serum albumin (BSA) and calf-thymus DNA (CT DNA) with UV–vis absorption, fluorescence, viscosity measurements and circular dichroism (CD) spectroscopies. The complexes exhibit good binding propensity to BSA and CT DNA. Both **1** and **2** have been found to promote cleavage of pUC19 DNA in the absence of any reducing agent. Antioxidant tests in vitro show the compounds possess significant antioxidant activity against superoxide and hydroxyl radicals.

1. Introduction

The phenazone-type pharmaceuticals dimethylaminophenazone (DMAA), metamizole, phenazone and propyphenazone have widely been used in medical care [1]. For example, phenazone is used as an analgesic either alone or in combination with other drugs. Furthermore, a great many phenazone complexes have also provoked a great interest in their diverse spectra of biological and pharmaceutical activities, such as antibacterial and antineoplastic activities [2]. In addition, metal complexes that bind and cleave DNA or proteins under physiological conditions are of current interests for their varied applications in nucleic acid and protein chemistry [3–7]. Transition metal complexes are being used at the forefront of many of these efforts. Stable, inert, and water-soluble complexes containing spectroscopically active metal centers are extremely valuable as probes for biological systems. Previous study revealed that transition metal complexes of the Schiff base of 4-amino-3-antipyrine show significant antibacterial activity [8]. However, the crystal structures and interactions with DNA or BSA of these complexes were not studied. At present, we synthesized the dinuclear (Co(II)) and mononuclear complex (Zn(II)) of the ligand 2, 6-di ((phenazonyl-4-imino) methyl)-4-methylphenol (Dpmp) which have different coordination geometry contrast to the reported structures. This may result in new biological activities. As we all know, serum albumins are proteins involved in the transport of metal ions and metal complexes with drugs through the blood stream [9,10]. Many drugs, including anticoagulants, tranquilizers, anti-inflammatory, and general anesthetics, are transported in the blood via combination with albumin [11]. The nature and magnitude of drug–albumin interactions significantly influence the pharmacokinetics of drugs, and the binding parameters are useful in studying protein–drug binding as they greatly influence absorption, distribution, metabolism, and excretion properties of typical drugs [11,12]. On the other hand, DNA is the material of inheritance and controls the structure and function of cells [13]. Binding studies of small molecules to DNA are very important in the development of DNA molecular probes and new therapeutic reagents. The study on the cleavage capacity of complex to DNA is considerably interesting as it can contribute to understanding their toxicity mechanism and to develop novel artificial nuclease. All these aroused our interest in the study of the new complexes of Dpmp with a view towards evaluating the binding behaviors of these compounds with CT DNA, BSA and exploring their anti-oxidative abilities.

In this paper, the ligand Dpmp and its dinuclear (Co(II)) and mononuclear (Zn(II)) complexes have been synthesized and characterized. The affinity of the complexes for BSA and CT DNA has been investigated. The DNA cleavage study was carried out at

* Corresponding author. Tel./fax: +86 931 8912582.
E-mail address: zengzhzh@yahoo.com.cn (ZhengZhi Zeng).

0223-5234/$ – see front matter © 2011 Elsevier Masson SAS. All rights reserved.
doi:10.1016/j.ejmech.2011.02.012

physiological pH and temperature. The anti-oxidative activity of the complexes has been evaluated by determining the IC_{50} values against the superoxide radicals ($O_2^{-\cdot}$) and Hydroxyl radicals ($OH^{\cdot}$).

2. Results and discussion

2.1. Synthesis and characterization of the complexes

The complexes were prepared by direct reaction of the ligand (Dpmp) with appropriate mole ratios of *M*(II) (*M* = Co and Zn) nitrate in ethanol. The transition metal complexes were stable in atmospheric conditions for extended periods, and are easily soluble in dimethylsulfoxide (DMSO), chloroform and N, N-dimethylformamide (DMF), partially in ethanol and methanol, and insoluble in water, benzene and ethylacetate. The IR spectra of the complexes are similar to the ligand. The bands at the 3456 cm^{-1} is ν(−OH) vibration in the ligand. In the complexes these bands are presented at 3430 and 3414 cm^{-1}, $\Delta\nu$ (ligand−complexes) is at 16 and 42 cm^{-1}. The ν(C═N) vibration of the free ligand Dpmp is at 1587 cm^{-1}; for the complexes these peaks appear at 1535 and 1538 cm^{-1}. The ν(C═O) vibration of the free ligand is at 1657 cm^{-1}; for the complexes these peaks appear at 1627 and 1635 cm^{-1}. These shifts demonstrate that the ketone oxygen and N atom of the C═N have formed a coordination bond with the metal ion. The band at 539 cm^{-1} for both complexes **1** and **2** is assigned to ν(*M*−O).

2.2. X-ray structure characterization

The X-ray crystallography data of complexes **1** and **2** were collected by the ω scan mode within $1.72° < \theta < 25.80°$ for *hkl* ($-12 \le h \le 9$, $-14 \le k \le 14$, $-15 \le l \le 17$) and $1.66° < \theta < 25.48°$ for *hkl* ($-9 \le h \le 12$, $-17 \le k \le 18$, $-24 \le l \le 24$), respectively. The complex **1** crystallized in a triclinic lattice with space groups $P-1$ while **2** in a monoclinic lattice with space group $P2(1)/n$. Each unit cell contains two or four molecules (Fig. S1).

For complex **1**, as Fig. 1a shows, it consists of $[Co_2(Dpmp)_2(NO_3)_2(H_2O)_2]^+$, a nitrate ion and an ethanol molecule. Single-crystal X-ray diffraction studies shows that the two Co atoms exhibit identical coordination environment, the metal centre allows the formation of a hexa-coordination environment with three oxygen atoms and one nitrogen atom from two Dpmp ligands, one oxygen atom of water molecule and the remaining one oxygen atom from the nitrate ion. The geometry can be described as a distorted octahedron (Fig. 1b). For O(1), O(2), N(3), O(7) and Co(1) atoms form the basal plane with Co(1)-O(1) 2.092(2), Co(1)-O(2) 2.019(2), Co(1)-N(3) 2.100(3) and Co(1)-O(7) 2.108(3) Å, the apical positions are occupied by O(4) with a Co(1)-O(4) distance of 2.169 (3) Å and O(3)A with a Co(1)-O(3)A distance of 2.194(2) Å.

For complex **2**, as Fig. 2a shows, it consists of a neutral [Zn (Dpmp)$(NO_3)_2$] unit. The zinc atoms in complex **2** have a hexa-coordinated geometry (Fig. 2b) with two oxygen atoms and one nitrogen atom of Dpmp and three oxygen atoms of two nitrate ions. The geometry can be described as a distorted octahedron. For O(1), O(2), O(4), O(7) and Zn(1) atoms form the basal plane with Zn(1)-O (1) 2.151(2), Zn(1)-O(2) 2.013(2), Zn(1)-O(4) 2.365(3) and Zn(1)-O (7) 2.032(3) Å, the apical positions are occupied by O(5) with a Zn (1)-O(5) distance of 2.050(2) Å and N(3) with a Zn(1)-N(3) distance of 2.194(2) Å.

2.3. Binding of serum albumins

2.3.1. Quenching mechanism of BSA fluorescence by *1* and *2*

Serum albumins, BSA and HSA, are most widely studied abundant proteins in plasma [14,15]. As the major soluble protein constituents of the circulatory system, they contribute to colloid

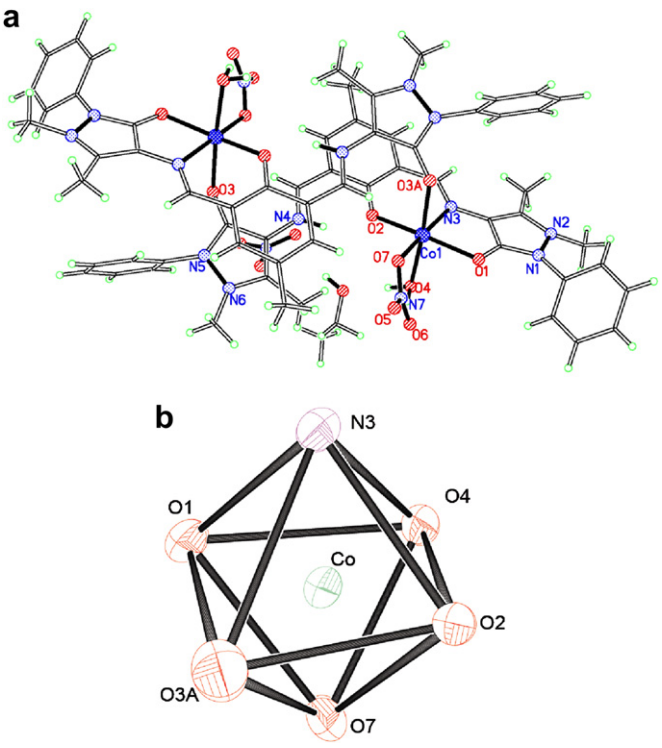

Fig. 1. The molecular structure and partially labeling of **1** (a); the coordination polyhedron of **1** (b).

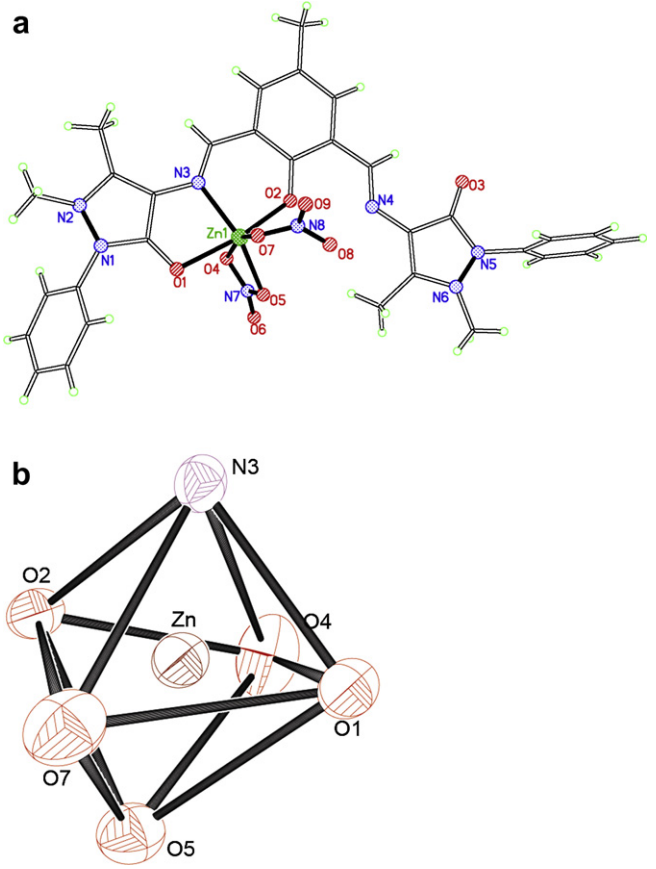

Fig. 2. The molecular structure and partially labeling of **2** (a); the coordination polyhedron of **2** (b).

osmotic blood pressure and are chiefly responsible for the maintenance of blood pH [16]. BSA is the most extensively studied serum albumin, due to its structural homology with HSA [17]. A useful feature of the intrinsic fluorescence of proteins is the high sensitivity of tryptophan and its local environment. Changes in the emission spectra of tryptophan are common in response to protein conformational transitions, subunit associations, substrate binding, or denaturation [17,18]. Therefore, the intrinsic fluorescence of proteins can provide considerable information on their structure and dynamics and is often utilized in the study of protein folding and association reactions. The interaction of the complexes with BSA has been studied from tryptophan emission–quenching experiments.

Addition of the complexes to BSA results in a significant decrease of the fluorescence intensity of BSA at 340 nm (Fig. 3), up to 72% of the initial fluorescence intensity of BSA for **1**, 55% for **2**, which indicates that there were interactions between the complexes and BSA. UV–vis spectra of BSA in the absence and presence of complexes **1** and **2** (Fig. S2) show that the absorption intensity of BSA was enhanced as the complexes increased, and there was a little blue shift. As is well known, dynamic quenching only affected the excited state of fluorophores but did not change the absorption spectrum. However, the formation of a non-fluorescence ground state complex induced a change in the absorption spectrum of fluorophores, therefore, the possible quenching mechanism of BSA by both complexes **1** and **2** are static quenching processes [19].

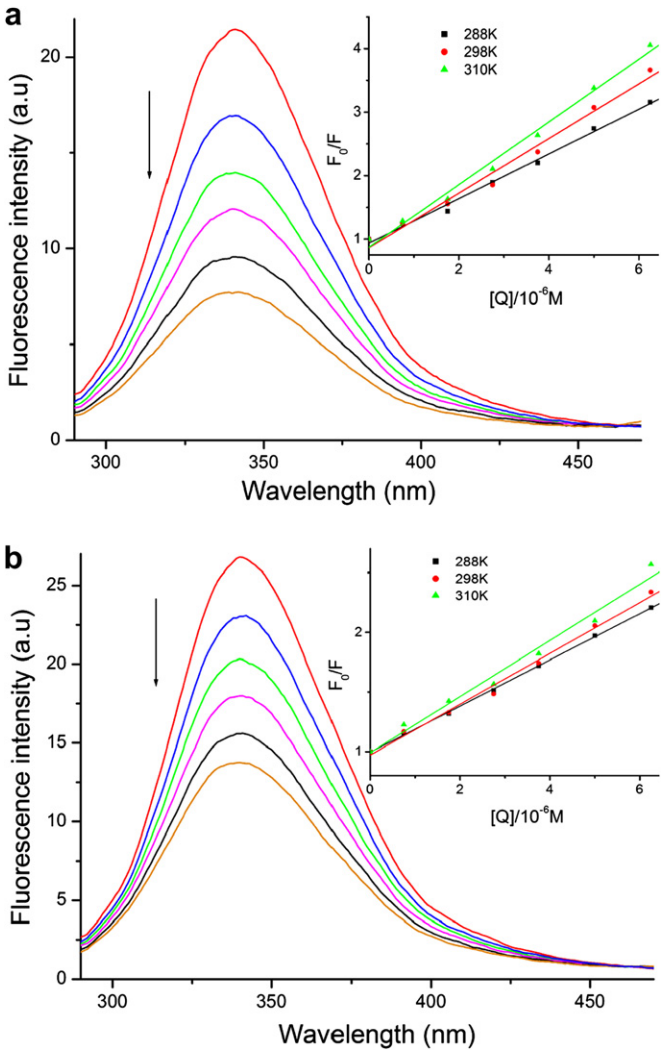

Fig. 3. Fluorescence spectra of BSA after excitation at 280 nm at pH 7.4 and 288 K at increasing amounts (0–6.25 μM) of the complexes (a) **1** and (b) **2**. The arrows show the changes upon increasing amounts of complex. Inset: plots of F_0/F for BSA against [Q] of the complex at different temperatures.

To elucidate further the quenching mechanism, fluorescence quenching data were analyzed with the Stern–Volmer equation. All of the Stern–Volmer plots of BSA-**1** and BSA-**2** systems at different temperatures follow a linear relation (inset in Fig. 3), this suggests that the quenching type was probably single quenching (static or dynamic quenching). The values for k_q (Table 1) are three orders of magnitude greater than the maximum diffusion collision quenching rate constant (2.0×10^{10} L mol^{-1} s^{-1}) for a variety of quenchers with biopolymers [20]. These results indicate that the quenching was not initiated from dynamic collision but static quenching. The binding constants K_A are increased with the rising temperature, which indicated that the stability of the state complexes increases with increasing temperature [21]. The K_{sv} value of **1** is larger than K_{sv} of **2** at any temperature, indicating that the interaction between **1** and BSA is stronger than **2**.

2.3.2. The binding parameters

Based on the plot of $\log(F_0 - F)/F$ versus $\log(1/([Dt] - (F_0 - F)[Pt]/F_0))$ (Fig. 4), the number of binding sites n and binding constant K_A can be obtained, as presented in Table 1. The values of n approximately equal to 1 indicate the existence of just a single binding site in BSA for the complexes.

Thermodynamic parameters for a binding interaction can be used as major evidence for the nature of intermolecular forces [22]. Among these parameters, the free energy change ΔG reflects the possibility of reaction, and the enthalpy change ΔH and entropy change ΔS are the main evidence for determining acting forces. To obtain such information, the thermodynamic parameters were calculated from the Van't Hoff equation. If $\Delta H \approx 0$, $\Delta S > 0$, the main force is a hydrophobic interaction; if $\Delta H < 0$, $\Delta S > 0$, the main force is an electrostatic effect; and if $\Delta H < 0$, $\Delta S < 0$, Van der Waals and hydrogen bond interactions play major roles in the reaction [23]. The values of thermodynamic parameters are shown in Table 1, where the negative sign for ΔG indicates the spontaneity of the binding of **1** and **2** with BSA. ΔH is small positive value and ΔS is positive value, indicating that the main binding force between the complexes and BSA is hydrophobic interaction.

According to the Förster nonradiative energy-transfer theory [24], the efficiency of energy transfer is E, the critical distance for 50% energy transfer is R_0, and the actual distance of separation is r. These values were calculated using Eqs. (1)–(3):

$$E = 1 - \frac{F}{F_0} = \frac{R_0^6}{R_0^6 + r^6} \tag{1}$$

$$R_0^6 = 8.78 \times 10^{-25} K^2 n^{-4} \phi_{\mathrm{Trp}} J \tag{2}$$

where K^2 is the orientation factor, ϕ_{Trp} is the quantum yield of the donor tryptophan in the absence of acceptor, n is the refractive index of the medium intervening between the donor and acceptor, and J is the spectral overlap integral defined by Eq. (3):

$$J = \sum F(\nu)\varepsilon(\nu)\nu^{-4}\Delta\nu / \sum F(\nu)\Delta\nu \tag{3}$$

where $F(\nu)$ is the fluorescence intensity of the donor, $\varepsilon(\nu)$ is the molar extinction coefficient of the acceptor in units of M^{-1} cm^{-1}, and ν is the frequency in cm^{-1}. The fluorescence emission spectrum of BSA and the UV absorption spectrum of **1** and **2** are shown in Fig. 5, which shows that they have some overlap. The value of

Table 1
Binding parameters for the BSA-complex system.

Complex		**1**			**2**	
T(K)	288 ± 0.2	298 ± 0.2	310 ± 0.2	288 ± 0.2	298 ± 0.2	310 ± 0.2
K_{sv} ($\times 10^5$ L mol^{-1})	3.60 ± 0.23	4.34 ± 0.13	5.47 ± 0.46	1.94 ± 0.04	2.19 ± 0.10	2.33 ± 0.01
K_q ($\times 10^{13}$ L mol^{-1} s^{-1})	3.60 ± 0.23	4.34 ± 0.13	5.47 ± 0.46	1.94 ± 0.04	2.19 ± 0.10	2.33 ± 0.01
K_A ($\times 10^5$ L mol^{-1})	4.49 ± 0.13	5.28 ± 0.07	6.09 ± 0.21	2.21 ± 0.06	2.34 ± 0.02	2.69 ± 0.13
n	0.95	1.04	0.99	0.92	0.87	0.79
R[a]	0.997	10.986	0.993	0.996	0.998	0.999
ΔG(kJ mol^{-1})	−31.16	−32.65	−34.43	−29.47	−30.63	−32.22
ΔH(kJ mol^{-1})		9.135			8.921	
ΔS(J mol^{-1} K^{-1})	139.91	140.22	140.21	134.20	132.72	132.71
E		0.2933			0.2471	
R_0 (nm)		3.27			2.81	
r (nm)		3.78			3.39	

[a] R is the correlation coefficient.

J for **1** was 4.4064×10^{-14} cm^{3}L mol^{-1} and for **2** was 1.791×10^{-14} cm^{3}L mol^{-1}. K^2 was taken as 2/3. n Was taken as 1.36 [24]. ϕ_{Trp} was determined in the study to be 0.15 [22]. With use of the values of J, K^2, n, and ϕ_{Trp}, the R_0, E and the actual distance r-value was calculated (Table 1). BSA has two tryptophan residues: Trp-212 is located in a hydrophobic fold and the additional tryptophan (Trp-134) is located on the surface of the molecule. In this study, the compounds were probably bound to the Trp-212 residue mainly through the hydrophobic interaction according to the thermodynamic results and the number of binding sites n. The actual distance r is 3.78 nm for **1** and 3.39 nm for **2**, indicating the energy transfer from BSA to **1** and **2** occurs with very high probability.

2.3.3. *Effects of **1** and **2** on BSA conformation*

Further experiments were carried out on the CD spectra to verify the binding process. As Fig. 6a shows, the CD spectra of BSA exhibited two negative bands in the UV region at 208 and 222 nm, characteristic of the α-helical structure of the protein [25]. The binding of complexes to BSA caused a decrease in band intensity in the ultra-UV CD, clearly indicating a decrease in the α-helical content in the protein. The average fractions of secondary structure estimated from the CD data are given in Table 2. The regular α-helix (α_R) content was 42.3% and the distorted α-helix (α_D) content was 22.9% in the BSA, while the α_R content was reduced to 37.4% and the distorted α_D content decreased to 17.6%, when the complexes bind to the complex **1**. For complex **2**, α_R and α_D contents are reduced to 40.1% and 21.5%, respectively. Moreover, the binding of the two complexes to BSA arouses the increase of the β-strand (β_R and β_D), turn (T), and unordered (U) structure. The calculated results exhibited a reduction of α-helix (α_R and α_D) structures from 65.2% to 55.0% for **1** and to 61.6% for **2** at the molar ratio complex/BSA of 1:1. The marked decrease probably occurred because of the strong interaction between the complexes and BSA, with the order **1** > **2**, which can be confirmed by the value of the binding constant K_A. This decreased helicity suggests that the binding of complexes with BSA induces a slight unfolding of the constitutive polypeptides of the protein, resulting in a conformational change in the protein which increased the exposure of some hydrophobic regions that were previously covered (Fig. 6b).

2.4. *Interaction with DNA*

2.4.1. *Fluorescence spectra*

The enhancements in the emission intensity of **1**, **2** and free ligand (Dpmp) with increasing CT DNA concentrations are shown in Fig. S3. In the absence of DNA, **1**, **2** and Dpmp emit weak luminescence in Tris buffer at ambient temperature, with a maximum appearing at 529 nm. When DNA is present the intensity of the emission for **1**, **2** and Dpmp all increase with respect to DNA concentration. This phenomenon is related to the extent to which the complexes penetrate into the hydrophobic environment inside the DNA, thereby avoiding the quenching effect of solvent water molecules. The marked increase in the emission intensity agrees with those observed for other intercalators [26].

2.4.2. *Electronic absorption titration*

UV spectroscopic titration is an effective method to examine the binding mode of DNA with metal complexes [27] since the observed changes of the spectra may give evidence of the existing interaction and its mode [28]. In general, hyperchromism and

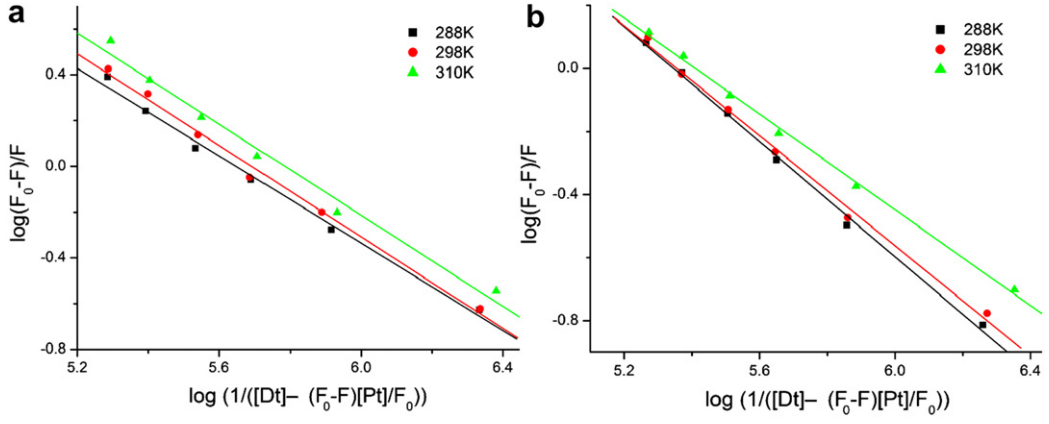

Fig. 4. Plots of $\log(F_0 - F)/F$ vs. $\log(1/([Dt] - (F_0 - F)[Pt]/F_0))$ for the BSA-complex system at different temperatures. (a) **1** and (b) **2**.

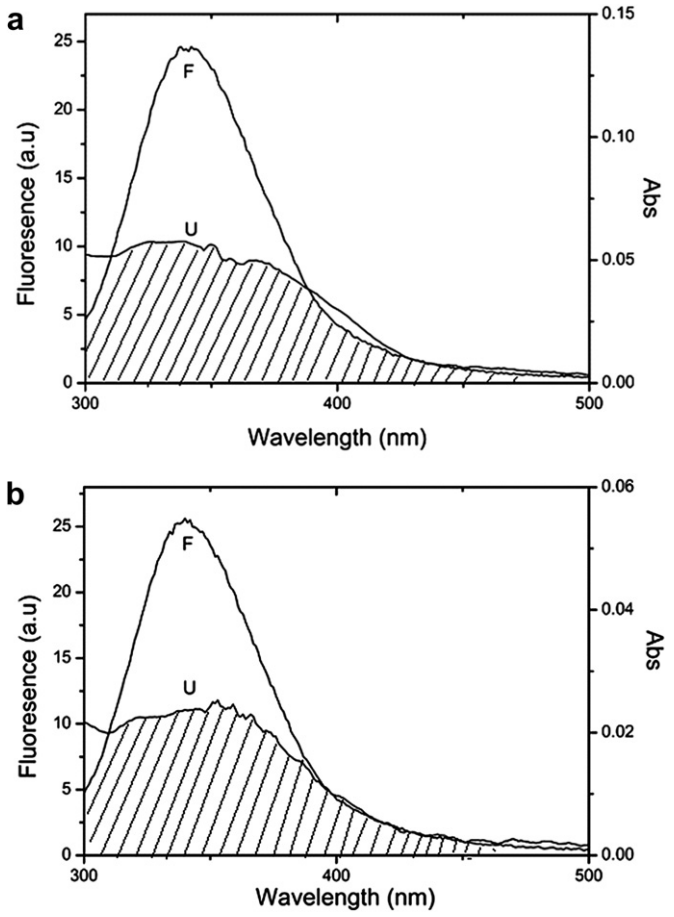

Fig. 5. Overlap of fluorescence spectra of BSA and UV absorption spectrum of (a) **1** and (b) **2**. F: Fluorescence spectrum of BSA (1.50 μM); U: UV absorption spectrum of the complexes (1.50 μM).

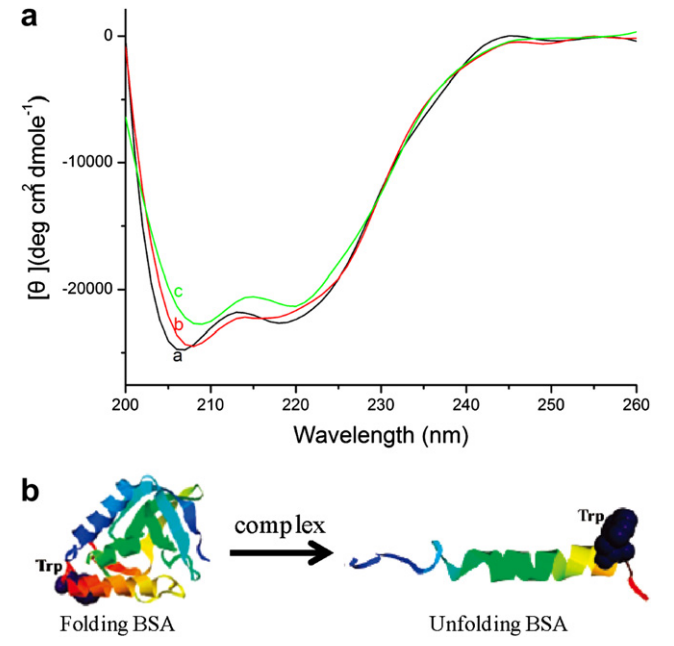

Fig. 6. (a) CD spectra of the BSA-complex system at room temperature (in cells of 1 mm path length). a: 1.50 μM BSA; b: 1.50 μM BSA + 1.5 μM **2**; c: 1.50 μM BSA + 1.5 μM **1**. (b) Schematic model showing the effect of ligands on the tryptophan environment in protein.

Table 2
Average estimates of the secondary structure fractions of BSA obtained with the CDPro software package after reaction with complexes **1** and **2**.

Compound	Fraction of secondary structure, %					
	α_R	α_D	β_R	β_D	T	U
BSA	42.3	22.9	5.5	4.2	7.1	18.1
BSA + **1**	37.4	17.6	6.1	6.4	10.5	22.6
BSA + **2**	40.1	21.5	5.6	4.4	9.1	19.3

hypochromism are the spectral features of DNA concerning changes of its double helix structure; hyperchromism means the breakage of the secondary structure of DNA and hypochromism shows that binding of complex to DNA can be due to electrostatic effect or intercalation which may stabilize the DNA duplex. Additionally, the existence of a red-shift is indicative of stabilization of DNA duplex [17,29]. The electronic absorption spectra of the ligand and its complexes **1**, **2** in the absence and presence of the CT DNA (at a constant concentration of the compounds) were obtained (Fig. 7). In the UV spectrum of Dpmp, **1** and **2**, the band centered at 335 nm exhibits a hypochromism of 13.4%, 30.1%, 49.4%, respectively. This indicates tight binding possibly by intercalation. K_b values of Dpmp, **1** and **2** were $1.60(\pm0.27) \times 10^5\ M^{-1}$, $8.02(\pm0.18) \times 10^5\ M^{-1}$ and $4.51(\pm0.31) \times 10^5\ M^{-1}$, respectively, (inset in Fig. 7). The K_b values of complexes are higher than that of ligand suggesting that the affinity of CT DNA is enhanced, when it is coordinated to Co(II) and Zn(II). It is noteworthy that the K_b values are higher than the binding affinity of EB for DNA, ($K_b = 1.23(\pm0.07) \times 10^5\ M^{-1}$) [30], suggesting that the existing interactions may cause EB displacement from its complex with DNA [30]. The competitive studies with EB are not carried since the ligand and complexes exhibit fluorescence emission at 545 nm when excited at 500 nm, which is close to the emission of DNA–EB system ($\lambda_{em} = 594$ nm). The results derived from the fluorescence and UV titration experiments suggest that both the ligand and complexes can bind tightly to CT DNA by intercalation.

2.4.3. Viscosity titration measurements

To further clarify the interactions between the studied compounds and CT DNA, viscosity measurements were carried out. Measurements of DNA viscosity that is sensitive to DNA length are regarded as the least ambiguous and the most critical tests of binding in solution in the absence of crystallographic structural data [31,32]. A classical intercalation mode demands that the DNA helix must lengthen as base pairs are separated to accommodate the binding complexes, leading to the increase of DNA viscosity, as for the behaviors of the known DNA intercalators [33]. In contrast, a partial and/or non-classical intercalation of the complex could bend (or kink) the DNA helix, reducing its viscosity concomitantly [34]. The effects of all the compounds on the viscosity of CT DNA are shown in Fig. S4. The viscosities of the DNA increase steadily with increasing concentrations of ligand and complexes **1** and **2**, and the extent of the increase observed for the ligand is smaller than that for complexes. Viscosity measurements clearly show that all the compounds can intercalate between adjacent DNA base pairs, causing an extension in the helix and thus increase the viscosity of DNA, and that the complexes can intercalate a little more strongly and deeply than the free ligand. The results obtained from the viscosity experiments validate those obtained from the spectroscopic studies.

2.4.4. Cleavage of pUC19 DNA

The study on the cleavage capacity of transition metal complex to DNA is considerably interesting as it can contribute to understanding the toxicity mechanism of them and to develop novel

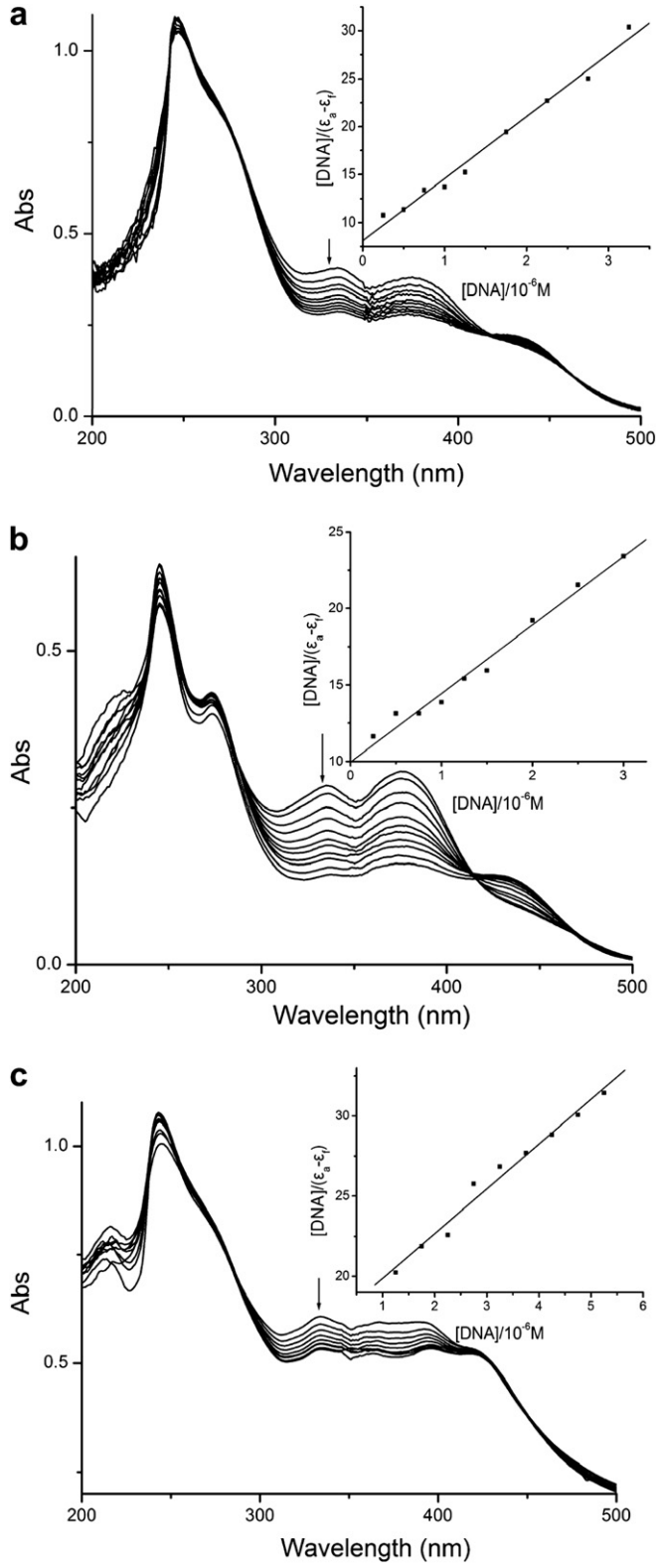

Fig. 7. UV spectra of (a) **1**, (b) **2** and (c) Dpmp ([compounds] = 10 μM) in DMF solution in the absence and presence of CT DNA ([CT DNA] = 0–5 μM) at increasing amounts. The arrows show the changes upon increasing amounts of CT DNA. Inset: plot of [DNA]/($\varepsilon_a - \varepsilon_f$) versus [DNA].

artificial nuclease. The cleavage ability of complexes **1** and **2** to pUC19 DNA was investigated by gel electrophoresis in Tris–HCl/NaCl buffer (pH 7.2) at 37 °C for 5 h. Both **1** and **2** show efficient DNA cleavage activity (Fig. 8). A 30 μM of **1** showed 95% cleavage of

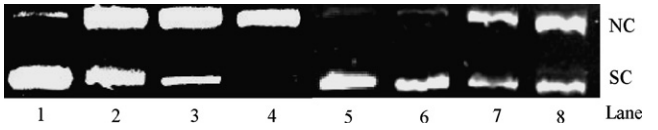

Fig. 8. Cleavage of pUC19 DNA (12 μM) by the complexes **1** and **2** in Tris–HCl/NaCl buffer (pH 7.2) at 37 °C for 5 h: lane 1: DNA control; lane 2: DNA + 10 μM **1**; lane 3: DNA + 20 μM **1**; lane 4: DNA + 30 μM **1**; lane 5: DNA control; lane 6: DNA + 10 μM **2**; lane 7: DNA + 20 μM **2**; lane 8: DNA + 30 μM **2**.

SC DNA to its nicked circular (NC) form, while 30 μM of **2** cleaved >60% of SC, the cleaved amount was enhanced with the increase of the concentration of the complex, showing the potential chemical nuclease activity of the complexes. Furthermore, **1** showed higher cleavage activity than **2** at the same concentration, which probably determined by **1** is a dinuclear complex but **2** is mononuclear. Therefore, hydrolytic cleavage of DNA because of high Lewis acidity of these metal ions probably occurred.

2.5. Anti-oxidative activity

Generation of reactive oxygen species (ROS) is a normal process in the life of aerobic organisms. Oxidative stress or excessive production of ROS is being implicated in many diseases [35]. ($O_2^{-\cdot}$) and ($OH^{\cdot}$) are two clinically important ROS in the human body [34]. They are produced in most organ systems and participate in various physiological and pathophysiological processes such as carcinogenesis, aging, viral infection, inflammation, and others [36]. Consequently, in this paper, the *M* (*M* = Cu and Zn) salts, the ligand and its complexes **1** and **2** were studied for their antioxidant activity by comparing their scavenging effects on $O_2^{-\cdot}$ and $OH^{\cdot}$. Fig. 9 shows the plots of suppression ratio (%) for $O_2^{-\cdot}$ and $OH^{\cdot}$, indicating that the average suppression ratio increases with increasing concentration of the compounds. The value of IC_{50} of Dpmp, **1** and **2** for $O_2^{-\cdot}$ are 49.2 μM, 39.1 μM and 55.8 μM, respectively, with the order of **2** > Dpmp > **1**. Complex **1** (IC_{50} = 39.1 μM) is the most effective of the three compounds for scavenging $O_2^{-\cdot}$. The order of IC_{50} for $OH^{\cdot}$ was **2** (50.9 μM) > **1** (43.1 μM) > Dpmp (30.1 μM). It is proved that the hydroxyl radical scavenging effects of ligand are higher than that of the complexes. Complex **1** was found to be a higher effective inhibitor for both $O_2^{-\cdot}$ and $OH^{\cdot}$ than **2**. This indicates a considerable potential for using them as inhibitor of the radical.

3. Conclusion

The synthesis and characterization of 2, 6-di ((phenazonyl-4-imino) methyl)-4-methylphenol and its Co(II) and Zn(II) complexes have been achieved with physicochemical and spectroscopic methods. Firstly, the binding behavior of the complexes with BSA was investigated under simulated physiologic conditions. The results showed that the intrinsic fluorescence of BSA was quenched by a static quenching mechanism and the complexes bound to BSA via hydrophobic interaction. The average binding distance between the complexes and BSA was obtained. The CD data indicate that the binding of **1** and **2** to BSA induces a conformational change in BSA. The complexes show good binding affinity to BSA giving relatively high binding constants. Therefore, the complexes can be deposited and transported by albumin. Secondly, the interaction of the complexes with CT DNA revealed that they can bind tightly to DNA probably via the intercalative mode. Complex **1** exhibits the highest K_b value, which is comparable to the K_b value of EB. Noticeably, both the two complexes have been found to promote cleavage ability of pUC19 DNA with the order **1** > **2**. The ligand and complexes showed

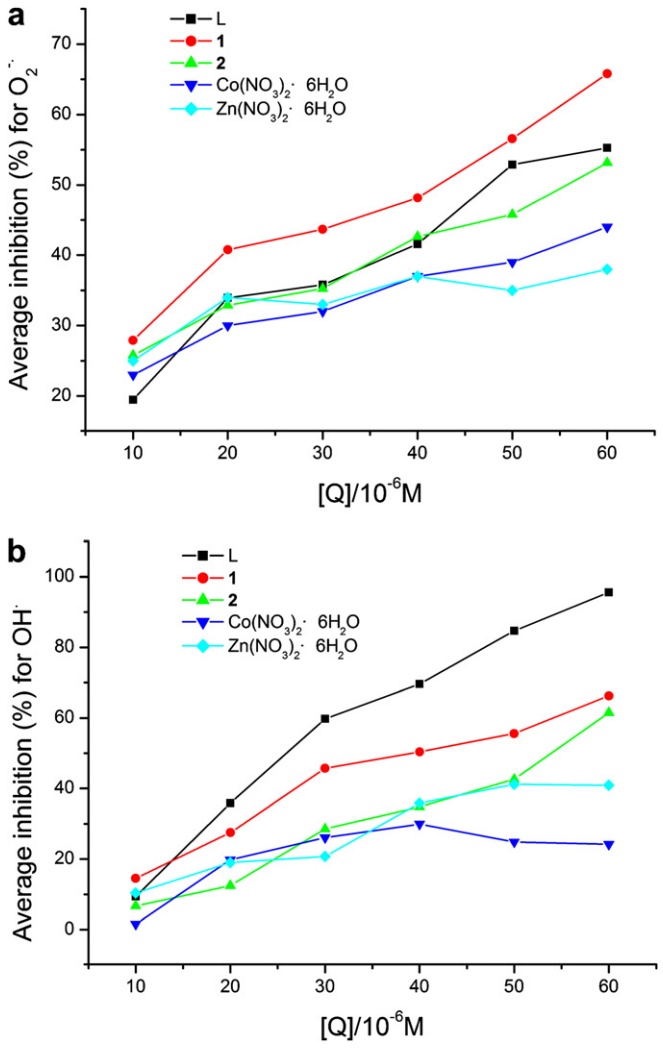

Fig. 9. Plots of the (a) superoxide radical scavenging effects (%) and (b) hydroxyl radical scavenging effects (%) for *M* (*M* = Co, Zn) salts Dpmp (*L*), **1** and **2**.

considerable anti-oxidative activity to $O_2^{-\cdot}$ and $OH^{\cdot}$, the suppression rate of **1** is greater than that of **2**. These findings clearly indicate that the complexes may have potential practical applications. Information obtained from our study would be helpful to understand the mechanism of interactions of phenazone-type pharmaceuticals and their complexes with serum albumin and nucleic acid and should be useful in the development of potential probes for BSA and DNA structure and conformation, or new therapeutic reagents for some certain diseases.

4. Experimental

4.1. Materials and instrumentation

All starting materials were of analytical grade and double-distilled water was used throughout the experiments. The reagents and solvents were purchased commercially and used without further purification unless otherwise noted. CT DNA, pUC19 DNA and BSA were obtained from Sigma Chemicals Co. (USA). Agarose was purchased from Promega Co. (German), ethidium bromide (EB) were obtained from Huamei Chemical Co. (Beijing, China). DNA stock solution was prepared by dilution of CT DNA to buffer (50 mM NaCl, 5 mM Tris–HCl (tris (hydroxymethyl) aminomethane hydrochloride) (pH 7.2)) followed by exhaustive stirring at 4 °C for three days, and kept at 4 °C for no longer than a week. BSA stock solution (1.50×10^{-5} mol L^{-1}) was kept in the dark at 0–4 °C. Tris/HCl buffer solution (pH 7.4) and NaCl solution (0.1 M) were prepared to maintain the ionic strength.

Carbon, hydrogen, and nitrogen were analyzed on an Elemental Vario EL analyzer. Infrared spectra (4000–400 cm^{-1}) were determined with KBr disks on a Thermo Mattson FTIR spectrometer. The UV–vis spectra were recorded on a Varian Cary 100 UV–vis spectrophotometer. The fluorescence spectra were recorded on a Hitachi RF-4500 spectrofluorophotometer. ^{1}H NMR spectra were measured on a Varian VR 300-MHz spectrometer, using TMS (tetramethylsilane) as a reference. Mass spectra were performed on a VG ZAB-HS Fast-atom bombardment (FAB) instrument and electrospray mass spectra (ESI-MS) were recorded on a LQC system (Finnigan MAT, USA) using DMF as mobile phase. CD measurements were performed on a Jasco-20 automatic recording spectropolarimeter (Japan) in cells of 1 mm path length at room temperature.

4.2. Synthesis of the ligand and complexes

4.2.1. Preparation of the ligand (L)

2, 6-Diformyl-4-methylphenol was prepared with the literature methods [37]. Then an ethanol solution containing 4-aminophenazone (2.03 g, 10 mmol) was added dropwise to a solution of 2, 6-diformyl-4-methylphenol (0.82 g, 5 mmol) in ethanol (150 ml). The mixture was stirred and heated to reflux for 3 h. The yellow precipitate was collected by filtration and washed with ethanol. The resulting Schiff base, 2, 6-di ((phenazonyl-4-imino) methyl)-4-methylphenol (Dpmp) was obtained (Scheme 1), which was dried under vacuum. Yield, 86%. Anal. Calcd. (%) for $C_{31}H_{30}N_6O_3$: C, 69.66; H, 5.62; N, 15.73. Found: C, 69.65; H, 5.37; N, 15.42. ^{1}H NMR ($CDCl_3$, 300 MHz, br, broad; s, singlet; m, multiplet): δ(ppm) 9.81 (2H, s, CH=N), 3.13 (6H, s, CH_3), 2.44 (6H, s, CH_3), 2.33 (3H, s, CH_3), 7.26–7.48 (12H, m, Ph–H). FAB MS: $m/z = 535.4$ ($M + H$). IR: ν_{max}(cm^{-1}): ν(C=O): 1657 cm^{-1}, ν(C=N): 1587 cm^{-1}, ν(C–N): 1295 cm^{-1}, ν(–OH): 3456 cm^{-1}. UV (DMF): λ_{max} (nm): 248, 337, 394, 420.

4.2.2. Preparations of the complexes

A 5 mL ethanol solution of $Co(NO_3)_2 \cdot 6H_2O$ (0.146 g, 0.5 mmol) was added slowly to a magnetically stirred 50 mL ethanol solution of the ligand (0.267 g, 0.5 mmol). The mixture was stirred in air for 4 h whereby a deep red solution was formed. It was filtered and kept in air. Red prismatic single crystals of Co(II) complex (**1**) suitable for X-ray crystallography were obtained on slow evaporation of the filtrate. The Zn(II) complex (**2**) was prepared by the same method using $Zn(NO_3)_2 \cdot 6H_2O$ instead ((Scheme 1)). Elemental Anal. Found (calculated) (%) for **1** $C_{33}H_{38}CoN_8O_{11}$ (%): C, 50.74 (50.66); H, 4.79 (4.96); N, 14.21 (14.33). IR for **1** (cm^{-1}): ν(C=O): 1623 cm^{-1}, ν(C=N): 1535 cm^{-1}, ν(C–N): 1293 cm^{-1}, ν(–OH): 3430 cm^{-1}. UV for **1** (DMF): λ_{max} (nm): 247, 332, 379. Elemental Anal. Found (calculated) for **2** $C_{31}H_{29}ZnN_8O_9$ (%): C, 51.29 (51.45); H, 4.12 (4.01); N, 15.63 (15.49). IR for complex **2** (cm^{-1}): ν(C=O): 1635 cm^{-1}, ν(C=N): 1538 cm^{-1}, ν(C–N): 1293 cm^{-1}, ν(–OH): 3414 cm^{-1}. UV for **2** (DMF): λ_{max} (nm): 244, 273, 334, 377.

4.3. Crystallography

Single-crystal X-ray diffraction collection was performed on a Rigaku RAXIS-RAPID diffractometer using a MoKα radiation (λ = 0.71073 Å). The structure was solved by direct methods. The positions of non-hydrogen atoms were determined from successive Fourier syntheses. The hydrogen atoms were placed in their geometrically calculated positions. The positions and anisotropic

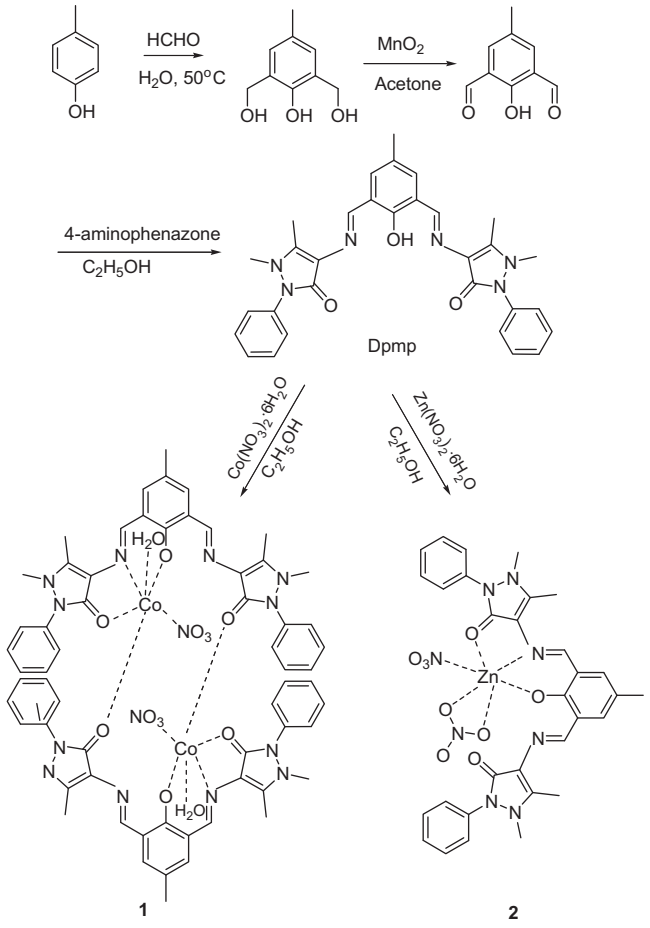

Scheme 1. A schematic depiction of the syntheses of the ligand and complexes.

thermal parameters of all non-hydrogen atoms were refined on F^2 by full-matrix least-squares techniques with the SHELX-97 program package [38]. Crystal data and details of the structure determination for **1** and **2** are summarized in Table 3. CCDC 787905 and CCDC 787906 contain the supplementary crystallographic data for this paper.

Table 3
Crystal data and structure refinement for complexes **1** and **2**.

	1	**2**
Empirical formula	$C_{33}H_{38}CoN_8O_{11}$	$C_{31}H_{29}ZnN_8O_9$
Formula weight	781.64	722.99
Temperature	296(2) K	296(2) K
Crystal system, space group	Triclinic, $P-1$	Monoclinic, $P2(1)/n$
a (Å)	10.5167(18)	10.136(3)
b (Å)	11.975(2)	15.372(4)
c (Å)	14.552(3)	20.568(6)
α (°)	88.532(3)	90
β (°)	78.160(3)	93.757(15)
γ (°)	80.733(3)	90
Volume (Å^3)	1770.3(5)	3197.9(14)
Z	2	4
Calculated density (g/cm^3)	1.446	1.502
Absorption coefficient (mm^{-1})	0.557	0.836
F(000)	814	1492
Crystal size (mm)	0.30 × 0.25 × 0.20	0.29 × 0.28 × 0.23
θ range for data collection (°)	1.72–25.80	1.66–25.48
Goodness-of-fit on F^2	1.015	0.995
Final R indices [$I > 2\sigma(I)$]	$R_1 = 0.0545$, $wR_2 = 0.1335$	$R_1 = 0.0458$, $wR_2 = 0.0779$
CCDC number	787905	787906

4.4. Albumin binding studies

In fluorometric titration experiments, 2.0 mL of operating solution (BSA 1.50×10^{-6} mol L^{-1}, NaCl 0.10 mol L^{-1}, pH 7.4) was titrated by successive additions of a 5.00×10^{-4} mol L^{-1} methanol stock solution of **1** and **2**. Titrations were done using a micro-injector, and the fluorescence intensity was measured (excitation at 280 nm and 5 nm slit widths) at three temperatures (288, 298, and 310 K). The temperature of samples was maintained with recycled water. The UV–vis spectrophotometer equipped with 1.0 cm quartz cells was used for scanning the UV spectrum in the wavelength range from 200 to 500 nm. The Tris/HCl buffer solution was used as a reference solution.

Fluorescence quenching data were analyzed with the Stern–Volmer Eq. (4) [39]

$$F_0/F = 1 + K_q\tau_0[Q] = 1 + K_{sv}[Q] \quad (4)$$

where F and F_0 are the relative fluorescence intensities in the presence and absence of quencher, respectively, [Q] is the concentration of quencher, K_{sv} is the Stern–Volmer quenching constant, k_q is the bimolecular quenching rate constant, τ_0 is the average bimolecular lifetime in the absence of quencher evaluated at about 10^{-8} s [40], f is the fraction of the initial fluorescence which is accessible to the quencher.

The apparent binding constant, K_A and binding sites n were evaluated using the following equation (Eq. (5)) [41]:

$$\log\frac{(F_0 - F)}{F} = n\log K_A - n\log\left(\frac{1}{[Dt] - (F_0 - F)[Pt]/F_0}\right) \quad (5)$$

where F_0 and F are the fluorescence intensities before and after the addition of the quencher, respectively, [Dt] and [Pt] are the total quencher concentration and the total protein concentration, respectively.

The values of ΔG, ΔH, and ΔS were calculated according to the data on the binding constant K_A at 288 K, 298 K, and 310 K using Eqs. (6)–(8).

$$\Delta G = -RT\ln K \quad (6)$$

$$\ln\frac{K_{A2}}{K_{A1}} = \left[\frac{1}{T_1} - \frac{1}{T_2}\right]\frac{\Delta H}{R} \quad (7)$$

$$\Delta G = \Delta H - T\Delta S \quad (8)$$

CD spectra (200–300 nm) were recorded at a BSA concentration of 1.50×10^{-6} mol L^{-1}, and the results were taken as molar ellipticity ([θ]) in deg cm^2 dmol^{-1}. In order to obtain the secondary structure fractions of BSA, the CDPro software package was used. This consists of the three programs, SELCON3, CONTIN, CDSSTR, and a program for determining tertiary structure class (CLUSTER). One of the major advantages of the CDPro software package is that the programs have been modified to accept any given set of reference proteins (CD spectra and secondary structure fractions), and seven such reference sets are provided. Moreover, input data files for these three programs are identical. More information about CDPro is available at the following website: http://lamar.colostate.edu/sreeram/CDPro [25].

4.5. Spectroscopic studies on DNA interaction

4.5.1. Electronic absorption spectra

The UV–vis absorbance at 260 and 280 nm of the CT DNA solution in 50 mM NaCl/5 mM Tris–HCl buffer (pH 7.2) give a ratio of ~1.9, indicating that the DNA was sufficiently free of protein

[42]. The DNA concentration was determined by measuring the UV absorption at 260 nm, taking the molar absorption coefficient (ϵ_{260}) of CT DNA as 6600 M^{-1} cm^{-1} [43]. The intrinsic binding constant K_b for the interaction of the studied complex with CT DNA was calculated by absorption spectral titration data using the following equation [44]:

$$[DNA]/(\varepsilon_a - \varepsilon_f) = [DNA]/(\varepsilon_b - \varepsilon_f) + 1/K_b(\varepsilon_b - \varepsilon_f) \quad (9)$$

where [DNA] is the concentration of DNA in base pairs, ε_a corresponds to the extinction coefficient observed (A_{obsd}/[complex]), ε_f corresponds to the extinction coefficient of the free compound which was calculated from the Lambert–Beer equation, ε_b is the extinction coefficient of the compound when fully bound to DNA, and K_b is the intrinsic binding constant. The ratio of slope to intercept in the plot of $[DNA]/(\varepsilon_a - \varepsilon_f)$ versus [DNA] gives the values of K_b. ε_f can be obtained from the intercept $1/K_b(\varepsilon_b - \varepsilon_f)$.

4.5.2. Fluorescence spectra

The complexes at a fixed concentration (10 μM) were titrated with increasing amounts of CT DNA. Excitation wavelength of the samples were 437 nm, scan speed = 240 nm/min, slit width 10/10 nm. All experiments were conducted at 20 °C in a buffer containing 5 mM Tris–HCl (pH 7.2) and 50 mM NaCl concentrations.

4.5.3. Viscosity experiments

Viscosity experiments were conducted on an Ubbelohde viscometer, immersed in a thermostated water-bath maintained at 25.0 °C. Titrations were performed for the complexes (1–5 μM), and each compound was introduced into DNA solution (5 μM) present in the viscometer. Data were presented as $(\eta/\eta_0)^{1/3}$ versus the ratio of the concentration of the compound and DNA, where η is the viscosity of DNA in the presence of compound and η_0 is the viscosity of DNA alone. Viscosity values were calculated from the observed flow time of DNA containing solution corrected from the flow time of buffer alone (t_0), $\eta = t - t_0$ [45,46].

4.6. DNA cleavage

The cleavage of supercoiled (SC) pUC19 DNA was studied by agarose gel electrophoresis, carried out in a dark room at 37 °C using SC DNA (2 μL, 12 μM) in Tris–HCl/NaCl buffer (pH 7.2) and the complex (2 μL) with varied concentrations. Each sample was incubated for 5.0 h at 37 °C and the cleavage reactions were quenched by the addition of bromophenol blue, then analyzed for the cleaved products using gel electrophoresis, in 0.8% agarose solution, at 5 V/cm for 40 min using TBE buffer [0.045 M tris (hydroxymethyl)aminomethane (tris), 0.045 M boric acid, and 1 mM EDTA, pH 7.2]. The gel was stained with 1 mg/ml ethidium bromide and photographed on an Alpha Innotech IS-5500 fluorescence chemiluminescence and visible imaging system.

4.7. Anti-oxidative activity

The superoxide radicals ($O_2^{-\cdot}$) were produced by the MET/VitB2/NBT system [47]. The amount of $O_2^{-\cdot}$ and suppression ratio for $O_2^{-\cdot}$ can be calculated by measuring the absorbance at 560 nm. The solution of MET, VitB2, and NBT were prepared in a 0.067 M phosphate buffer (pH = 7.8) while avoiding light. The tested compounds were dissolved in DMF. The 5 mL reaction mixture contained MET (0.01 M), NBT (4.6×10^{-5} M), VitB2 (3.3×10^{-6} M), and the tested compound. After illuminating the solution with a fluorescent lamp at 30 °C for 30 min, the absorbance (A_i) of the samples was measured at 560 nm. The sample without the tested compound was used as the control and its absorbance was used as A_0. The suppression ratio for $O_2^{-\cdot}$ was calculated from the following Eq. (10):

$$\text{Suppression ratio} = (A_0 - A_i)/A_0 \quad (10)$$

where A_i is the absorbance in the presence of the ligand or its complexes and A_0 is the absorbance in the absence of the ligand or its complexes.

Hydroxyl radical ($OH^{\cdot}$) scavenging activity through the Fenton reaction [48]. The solution of the compound to be tested was prepared in DMF. The tested samples contained 1 mL of 0.15 M phosphate buffer (pH = 7.4), 1 mL of 40 μg/mL safranin, 1 mL of 1.0 mM EDTA-Fe(II), 1 mL of 3% H_2O_2, and 0.5 mL of the solution of the tested compound (prepared as a series dilutions of the tested compound). The reaction mixtures were incubated at 37 °C for 60 min in a water-bath. The absorbance of the samples and a control were measured at 520 nm. The suppression ratio for $OH^{\cdot}$ was calculated from the following Eq. (11) [49].

$$\text{Suppression ratio} = (A_{sample} - A_{blank})/(A_{control} - A_{blank}) \quad (11)$$

where A_{sample} is the absorbance of the sample in the presence of the tested compound, A_{blank} is the absorbance of the blank in the absence of the tested compound and $A_{control}$ is the absorbance in the absence of the tested compound and EDTA-Fe(II). IC_{50} value was introduced to denote the molar concentration of the tested compound which caused good inhibitory or scavenging effect on radicals.

Acknowledgment

This study was supported by the Foundation of Key Laboratory of Nonferrous Metals Chemistry and Resources Utilization of Gansu Province and State Key Laboratory of Applied Organic Chemistry and the NSFC (20171019).

Appendix. Supplementary material

Supplementary material can be found, in the online version, at doi: 10.1016/j.ejmech.2011.02.012.

References

[1] S. Zuehlke, U. Duennbier, T. Heberer, Chemosphere 69 (2007) 1673–1680.
[2] M.M. Girges, M.M. Abou El-Zahab, M.A. Hanna, Arch. Pharm. Res. 11 (1988) 169–174.
[3] S.J. Franklin, Curr. Opin. Chem. Biol. 5 (2001) 201–208.
[4] J.A. Cowan, Curr. Opin. Chem. Biol. 5 (2001) 634–642.
[5] T.D. Maurer, B.J. Kraft, S.M. Lato, A.D. Ellington, J.M. Zaleski, Chem. Commun. (2000) 69–70.
[6] E. Meggers, Chem. Commun. (2009) 1001–1010.
[7] Q. Saquib, A.A. Al-Khedhairy, S. Al-Arifi, A. Dhawan, J. Musarrat, Toxicol. In. Vitro. 23 (2009) 848–854.
[8] S.M. Annigeri, M.P. Sathisha, V.K. Revankar, Transit. Met. Chem. 32 (2007) 81–87.
[9] Z. Ma, F.E. Jacobsen, D.P. Giedroc, Chem. Rev. 109 (2009) 4644–4681.
[10] A. Atkinson, D.R. Winge, Chem. Rev. 109 (2009) 4708–4721.
[11] A. Sułkowska, M. Maciaek-Jurczyk, B. Bojko, J. Mol. Struct. 881 (2008) 97–106.
[12] F. Zsila, Z. Bikádi, M. Simonyi, Biochem. Pharmacol. 65 (2003) 447–456.
[13] Y.T. Sun, S.Y. Bi, D.Q. Song, C.Y. Qiao, D. Mu, H.Q. Zhang, Sens. Actuators. B. Chem. 129 (2008) 799–810.
[14] D.C. Carter, B. Chang, J.X. Ho, K. Keeling, Eur. J. Biochem. 226 (1994) 1049–1052.
[15] J.R. Brown, P. Shockley, Lipid–Protein Interactions, vol. 1, Wiley Interscience, 1982, pp. 25–68.
[16] F. Tan, M. Guo, Q.S. Yu, Spectrochim. Acta Part A. 61 (2005) 3006–3012.
[17] E.K. Efthimiadou, A. Karaliota, G. Psomas, J. Inorg. Biochem. 104 (2010) 455–466.
[18] A. Sulkowska, J. Mol. Struct. 616 (2002) 227–232.
[19] X.W. Zhang, F.L. Zhao, K.A. Li, Chem. J. Chin. Univ. 20 (1999) 1063–1067.

[20] C.Q. Jiang, M.X. Gao, J.X. He, Anal. Chim. Acta. 452 (2002) 185–189.
[21] H. Xu, Q. Liu, Y. Wen, Spectrochim. Acta Part A. 71 (2008) 984–1988.
[22] H.Y. Liu, Z.Z. Xu, X.H. Liu, P.X. Xi, Z.Z. Zeng, Chem. Pharm. Bull. 57 (2009) 1237–1242.
[23] P.D. Ross, S. Subramanian, Biochemistry 20 (1981) 3096–3102.
[24] W.DeW. Horrocks, W.E. Collier, J. Am. Chem. Soc. 103 (1981) 2856–2862.
[25] F.J. Chen, G.Q. Liu, Z.H. Xu, Z.Z. Zeng, Biochem. Mol. Biol. Int. 41 (2008) 305–1309.
[26] A. Nohara, T. Umetani, Y. Sanno, Tetrahydron Lett. 14 (1973) 1995–1998.
[27] J.K. Barton, A.L. Raphael, J. Am. Chem. Soc. 106 (1984) 2172–2176.
[28] H. Chao, W. Mei, Q. Huang, L. Ji, J. Inorg. Biochem. 92 (2002) 165–170.
[29] E.C. Long, J.K. Barton, Acc. Chem. Res. 23 (1990) 271–273.
[30] A. Dimitrakopoulou, C. Dendrinou-Samara, A.A. Pantazaki, M. Alexiou, E. Nordlander, D.P. Kessissoglou, J. Inorg. Biochem. 102 (2008) 618–628.
[31] S. Mahadevan, M. Palaniandavar, Inorg. Chem. 37 (1998) 693–700.
[32] A.B. Tossi, J.M. Kelly, Photochem. Photobiol. 9 (1989) 545–556.
[33] J.G. Liu, Q.L. Zhang, X.F. Shi, L.N. Ji, Inorg. Chem. 40 (2001) 5045–5050.
[34] S. Satyanarayana, J.C. Dabrowiak, J.B. Chaires, Biochemistry 32 (1993) 2573–2584.
[35] K.V. Sashidhara, A. Kumar, G. Bhatia, M.M. Khan, A.K. Khanna, J.K. Saxena, Eur. J. Med. Chem. 44 (2009) 1813–1818.
[36] A.M. Pyle, J.P. Rehmann, R. Meshoyrer, C.V. Kumar, N.J. Turro, J.K. Barton, J. Am. Chem. Soc. 111 (1989) 3051–3058.
[37] N.V. Verani, E. Rentschler, T. Weyhermuller, E. Bill, P. Chaudhuri, J. Chem. Soc., Dalton Trans. (2000) 251–258.
[38] G.M. Sheldrick, SHELXTL v5, Reference Manual, Siemens Analytical X-ray Systems, Madison, WI, 1996.
[39] S.S. Lehrer, Solute perturbation of protein fluorescence, Biochemistry 10 (1971) 3254–3263.
[40] J.R. Lakowicz, G. Weber, Biochemistry 12 (1973) 4171–4179.
[41] S.Y. Bi, L. Ding, Y. Tian, J. Mol. Struct. 703 (2004) 37–45.
[42] J. Marmur, J. Mol. Biol. 3 (1961) 208–218.
[43] M.F. Reichmann, S.A. Rice, C.A. Thomas, P. Doty, J. Am. Chem. Soc. 76 (1954) 3047–3053.
[44] A. Wolf, G.H. Shimer, T. Meehan, Biochemistry 26 (1987) 6392–6396.
[45] R.T. Mostafa, H.M. Seyed, R. Bijan, Biochem. Mol. Biol. Int. 39 (2006) 530–536.
[46] S. Zahra, H. Saman, R. Bijan, N.G. Mohsen, Biochem. Mol. Biol. Int. 39 (2006) 636–641.
[47] C.C. Winterbourn, Biochem. J. 182 (1979) 625–628.
[48] C.C. Winterbourn, Biochem. J. 198 (1981) 125–131.
[49] Z.Y. Guo, R.E. Xing, S. Liu, H.H. Yu, P.B. Wang, C.P. Li, P.C. Li, Bioorg. Med. Chem. Lett. 15 (2005) 4600–4603.